

Cascaded silicon-on-insulator microring resonators for the detection of biomolecules in PDMS microfluidic channels

Jonas Flueckiger*, Samantha M. Grist, Gural Bisra, Lukas Chrostowski, Karen C. Cheung
Department of Electrical and Computer Engineering, The University of British Columbia
2332 Main Mall, Vancouver, BC, Canada, V6T1Z4

ABSTRACT

Silicon-On-Insulator (SOI) photonic microring resonators have shown promising potential for real time detection of biomolecules because of the sensitivity towards surface binding events. Previous work shows the use of single ring resonators for sensing applications. Each ring requires an input and output coupler and can be addressed only one at a time. We propose a novel use of cascaded ring resonators (width $w = 200$ nm and bending Radius $R = 30$ μm) together with a PDMS microfluidic network fabricated by soft lithography to expose each ring individually with different solutions. The SOI substrate with the planar waveguides and the PDMS with the microchannels are reversibly bonded to each other. The use of cascaded ring resonators offers the possibility to measure transmission spectra of multiple rings in different channels simultaneously. We measured Q-factors of $>30'000$ in air and $>10'000$ when exposed to water. Using a water/glycerin solution with known refractive indices we determine the sensitivity to be ~ 40 nm/RIU.

Keywords: Nanophotonics, Label-free biosensors, Silicon-on-insulator, Ring Resonator, Microfluidics

1. INTRODUCTION

Evanescent field sensors such as Surface Plasmon Resonance (SPR) or planar waveguide based sensors are amongst the most popular optical detection techniques for sensitive and label free biomolecular detection¹. Silicon-On-Insulator (SOI) photonic microcavity resonators have shown promising potential for real time detection of biomolecules because of their sensitivity towards surface binding events. Traditionally, these resonators have been demonstrated in add-drop filter²⁻³, optical switches⁴, and laser applications⁵⁻⁶. It has been shown that silicon-on-insulator (SOI) waveguides with dimensions smaller than the wavelength of light have a strong evanescent field at the waveguide surface extending a few hundred nanometers into the surrounding media. Any interaction with molecules in proximity or surface bound molecules will change the effective refractive index of the guided mode and thus alter the resonance behavior. The degree of interaction of the evanescent field and the sample is limited by the number of roundtrips by the light inside the ring and the footprint of the sensing area can be reduced without losing sensitivity. In case of a straight waveguide based sensor, such as a Mach-Zehnder the interaction is limited by the physical length of the sensing waveguide. Optical sensors based on ring and racetrack resonators have been proposed and developed using a variety of materials and for a variety of applications such as chemical sensing⁷⁻⁸ and sensing of biological molecules such as antibodies or antigens⁹⁻¹². In particular, the optical, label-free detection of biomolecules is a topic of considerable interest¹³⁻¹⁴. The sensitivity of a ring resonator is dependent on the overlap of the evanescent field and the sample¹⁵. In a strip waveguide most of the power is contained inside the core and only a small portion propagates outside in the media. To further enhance the sensitivity, slotted waveguides^{8, 16-20} or resonator disks²¹ have been used. Compared to other sensing methods, optical sensors methods have the advantages of high sensitivity, no physical contact, immunity to electromagnetic interference, and multiplexed interrogation.

The most basic configuration of a ring or racetrack resonator sensor is to couple the light to individual input and output optical fibers. A vertical-to-horizontal grating coupler design (70 nm trenches) is used for TE-like optical mode injection. It is of interest to integrate multiple resonators on a single chip to perform multiple measurements in parallel or to compensate for temperature drifts²². By using the basic configuration, the required number of input and output fibers increases proportionally with each added resonator and parallel measurement can only be done with sophisticated measurement and alignment set ups. Ramachandran *et al.* integrated 5 resonators on a single chip each of those resonators connected individually to input/output optical fibers⁹. Kwon *et al.* use two cascaded polymer microring resonators on the

*Corresponding author: jonasf@ece.ubc.ca

same straight waveguide fabricated out of Su-8²³. One resonator was covered by a cladding and the second resonator was exposed to the analytes. The covered resonator was used to compensate for temperature drifts. Dai *et al.* amongst others investigated the use of cascaded resonators theoretically²⁴⁻²⁶. Gylfason *et al.* used a multi-mode interference splitter integrated on the same chip as the resonators to address 8 rings using only one input grating coupler²². The waveguide's output is focused onto a single pixel photodiode array. The resonators are etched into a silicon nitride film on top of silicon oxide layer.

The concept of a lab-on-a-chip combines sample handling and analysis in one single chip, thereby offering the possibility of a portable analysis platform. Picoliter sample volumes can be handled inside micrometer scale fluidic channels using valves and pumps integrated into silicon or polymer chips²⁷. It is of great interest to include sensor technology into these lab-on-chip devices to automate parallel processing and therefore lower cost and increase throughput. Ksendzov *et al.* clamped a flow cell down onto the sensor chip²⁸. They achieved sealing by using an o-ring and pressure. However they are not able to expose individual resonators with different analytes. Washburn *et al.* and Luchansky *et al.* used a laser cut Mylar gasket aligned over top of the microring arrays to define microfluidic channels^{1, 11}. They closed the channels off with a Teflon lid and sandwiched the different layers between an aluminum chip holders. These microwells are only useful for steady state measurements. Because mass transport is diffusion limited, they are not suitable to determine dynamics of fast reactions, e.g. binding events of proteins. Moreover, in order to be able to run several experiments with different analytes or different concentrations in parallel individual resonators need to be addressed and exposed. Carlborg *et al.* used a microfluidic channel network in poly(dimethylsiloxane) (PDMS), with a separate fluid channel to each sensor for sample delivery¹⁰.

We propose the use of cascaded ring resonators together with a PDMS microfluidic network fabricated by soft lithography to expose each ring individually with different solutions. The SOI substrate with the planar waveguides and the PDMS with the microchannels are reversibly bonded to each other. The use of cascaded ring resonators offers the possibility to measure transmission spectra of multiple rings in different channels simultaneously. The volume refractive index sensitivity of the racetrack resonator is determined by injecting a water – glycerin mixture with different mixing ratios and known refractive indices.

2. MATERIALS AND METHODS

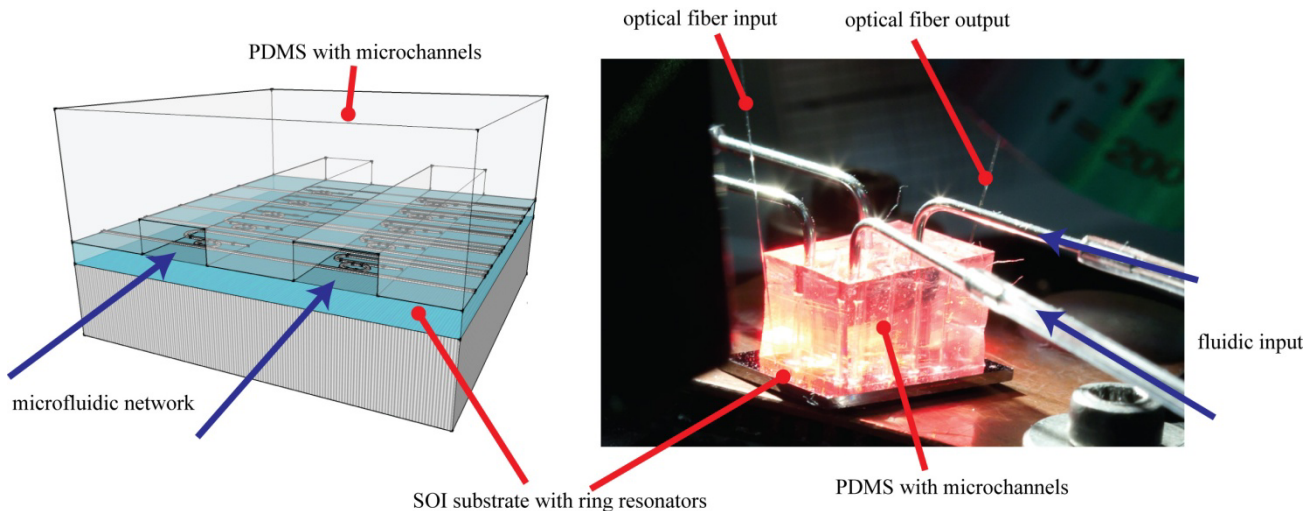


Figure 1. The measurement setup: the optical input fiber is connected to a tunable laser source with wavelength at around 1550 nm and the output optical fiber is connected to an optical power sensor. The measurements are performed on a temperature controlled stage. Fluidic tubing are connected to a syringe pump.

2.1 Fabrication of SOI ring resonators

The SOI nanophotonic single-mode waveguides were fabricated with deep UV lithography (193 nm) and standard CMOS etching processes as part of IMEC's passive photonic ePIXfab cSOI process. It is possible to get features down

to 120 nm and a minimum pitch of 300 nm. The ring/racetrack resonators are patterned onto a 200 mm SOI wafer. The buried oxide layer is 2000 nm thick and the crystalline top silicon film is 220 nm thick. A vertical-to-horizontal grating coupler design (70 nm trenches) is used for TE-like optical mode injection. The straight waveguides have a width of $w = 500$ nm. The design includes several configurations with 1-4 cascaded rings or racetracks with different radii and different coupling gaps. DW-2000 mask layout design software from Design Workshop technologies, Quebec, Canada was used to design the resonator mask layout.

2.2 Fabrication of PDMS microfluidic device

PDMS is the most widely used polymer in the field of microfluidics. It is a biocompatible, transparent, rubber-like polymer and can be easily patterned using soft lithography, a well established fabrication method. The mold masters were fabricated with standard photolithography techniques on Su-8 2075 (MicroChem, USA). Through replica molding the patterns were transferred onto PDMS. The uncured PDMS (Sylgard 184, Dow Corning USA) was poured onto the mold master to a thickness of about 1 cm, degassed to remove air bubbles, and cured at 80 °C for 2h on a hotplate. The hydrophobic surface properties can be altered in an oxygen plasma by replacing some of the surface methyl groups (CH_3) by a hydroxyl groups ($-\text{OH}$). This activated surface can form covalent siloxane bonds (Si-O-Si) when in contact with glass or silicon substrates, forming an irreversible seal. After punching access holes for the fluidic inlet and outlets the PDMS layer and the resonator substrate were aligned and bonded to each other.

2.3 The measurement set up

A tunable laser source (Agilent 81681A, Agilent Technologies, Inc., USA) was used with an output wavelength range from 1460 nm to 1580 nm. A single mode optical fiber was aligned with the vertical-to-horizontal grating coupler design to inject light into the SOI waveguides. The output light intensity was collected with a multimode optical fiber and measured with an optical power sensor (Agilent 81635A, Agilent Technologies, Inc., USA). The temperature of the substrate was kept constant with a Peltier element and a temperature controller (Stanford Research System, USA) in a closed feedback loop configuration.

3. FINITE ELEMENT MODELLING

The resonators were simulated using Lumerical MODE Solutions and a custom MATLAB script. MODE Solutions was used to simulate the mode profiles, effective refractive indices, and material losses for a straight SOI waveguide, bent waveguides, and coupler regions. This data was then imported into a custom MATLAB script to simulate the resonator response. Due to fabrication process parameter variations, the cross-sections of the waveguides are trapezoidal instead of the desired rectangular shape. The finite element model takes these aberrations into account as presented in 3.1. The simulation procedure and results for the mode profiles are presented in 3.2, while the MATLAB script simulation procedure and results for a single refractive index and simulated shifts in refractive index are presented in 3.3 and 3.4, respectively.

3.1 Corrections for Fabrication Errors

In an effort to accurately simulate the waveguide geometry and account for any discrepancies between fabrication and design, Scanning Electron Microscope (SEM) images were taken of the design. In order to image the waveguide cross-section and estimate the sidewall slope of the waveguides, a Focused Ion Beam (FIB) was used to mill trenches over a straight waveguide as well as two coupler regions (one of 200 nm waveguide spacing and the other of 400 nm waveguide spacing). After FIB milling, the waveguides were imaged with a 52° tilt to observe their cross-sections. The pixel lengths of the waveguides were then compared with the pixel length of the scale bar to determine the widths of the top and bottom of the waveguides; the coupler gaps were determined with a similar method. The average of five measurements was used as the waveguide dimensions for simulation. Only one measurement was obtained for each of the coupler gaps. It was determined that the 220 nm (as verified by profilometry) silicon layer was approximately 470 (± 17) nm wide at the top edge and 575 (± 11) nm wide at the SiO_2 interface, indicating a sidewall angle of approximately 14° ($\pm 2^\circ$). The coupler gaps at the SiO_2 interface were determined to be approximately 113 nm for the 200 nm coupler gap design and 327 nm for the 400 nm coupler gap design.

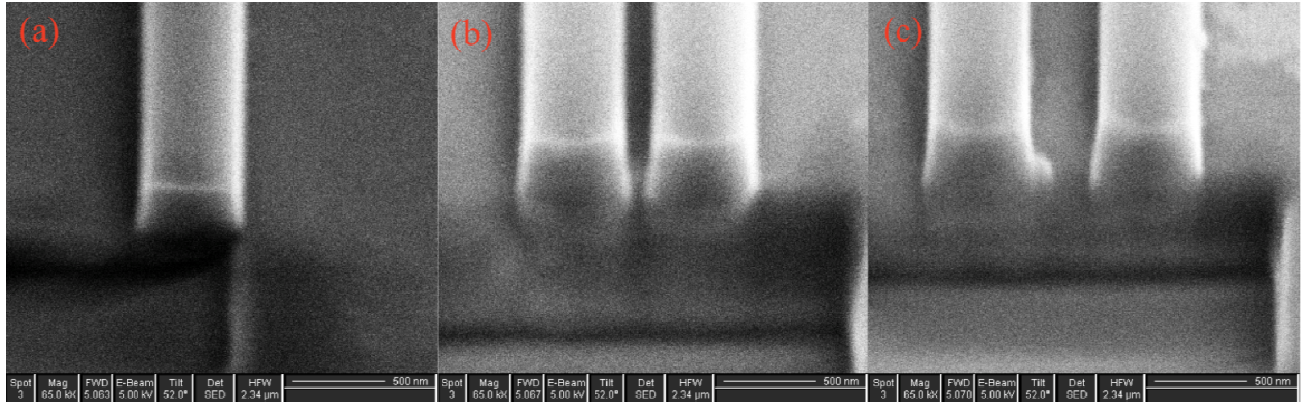


Figure 2. The SEM images of the FIB-milled waveguide cross-sections used to measure the waveguide dimensions. All three images were taken at 65 kx magnification with a 52° tilt and the scale bar at the bottom of each image represents 500 nm. (a) Single waveguide. (b) Directional coupler with 200 nm coupler gap. (c) Directional coupler with 400 nm coupler gap.

3.2 Simulated Mode Profiles

The waveguide and coupler geometries presented in 3.1 were imported into Lumerical MODE Solutions to simulate the mode profiles. The waveguides and SiO₂ substrate were modeled using the default MODE Solutions material files for silicon and silicon dioxide. The surrounding media was simulated by either using the default MODE Solutions material file for water or slightly modifying it to achieve a constant offset in the real part of the refractive index due to the addition of glycerin. The offset used is presented in table 1.

Table 1: Refractive index of Glycerin-Water solutions at 20°C.

Glycerin % by Weight	Refractive Index n
0	1.33303
5	1.33880
10	1.34481
15	1.35106
20	1.35749

The mode profiles were first simulated for an incident wavelength of 1500 nm, and then the mode was tracked over varying wavelengths. A 10-point frequency sweep was first obtained for a straight waveguide and it was determined that the effective index (n_{eff}) varied approximately linearly over this wavelength range. To conserve resources, each of the subsequent measurements were only measured at 1500 nm and 1600 nm, and the group index (n_g) was determined from the slope between these datapoints. Because the wavelength dependence and imaginary part of the refractive index of the medium was assumed to be the same for pure water and various water-glycerin concentrations, the same wavelength dependence of the effective refractive index and the same material loss were used for all of the simulated media.

MODE Solutions profiles were obtained for coupler regions corresponding to both of the resonator’s directional couplers and bent waveguides of the appropriate bend radii. Each of these simulations was repeated for various water - glycerin concentrations tested, and the detailed mode data were exported to text files. The mode crossover loss between the straight and curved waveguide sections was also simulated for each bend radius.

The mode profiles for the straight waveguide and two directional couplers (200 nm and 400 nm gap spacing) are presented in Figure 3.

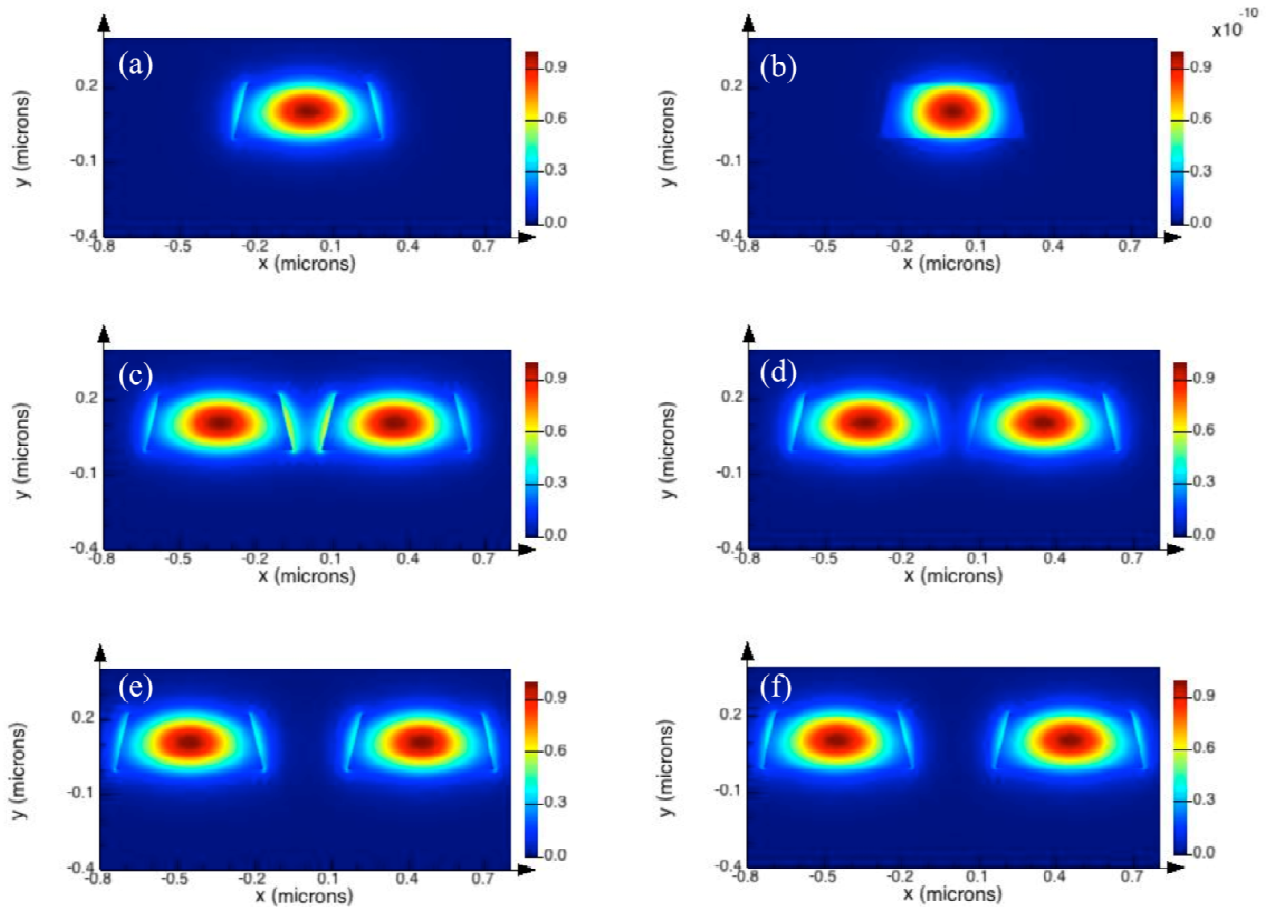


Figure 3: Mode profiles simulated using Lumerical MODE Solutions. (a) shows the electric field intensity profile for a straight waveguide, (b) shows the energy density profile for a straight waveguide, (c) and (d) depict the electric field intensities for the two supermodes of the 200 nm gap spacing coupler, and (e) and (f) depict the electric field intensities for the two supermodes of the 400 nm gap spacing coupler

3.3 Simulated Transmission Spectra

After simulation, the MODE Solutions data were imported into a custom MATLAB script to simulate the resonator responses from analytical models. This script used the effective indices and material losses determined from the mode profiles to determine the phase difference (δ) and losses (α) resulting from a round trip of the resonator as well as the field coupling (κ) and transmission (t) for each of the resonator's directional couplers. The script employed analytic functions previously presented by our group²⁹ to determine these values.

The resonator response was then simulated from these values using the analytical model for a double-bus ring resonator shown in equation 1³⁰L

$$E_{through} = \frac{t_1 - t_2^* \alpha e^{i\delta}}{1 - t_1^* t_2^* \alpha e^{i\delta}}, \quad (1)$$

where the subscripts on the values for field transmission refer to the through port coupler (t_1) and the add/drop port coupler (t_2). The simulated transmission spectra for two cascaded racetrack resonators with slightly different free spectral ranges (FSR) are presented in Figure 4 together with measured data.

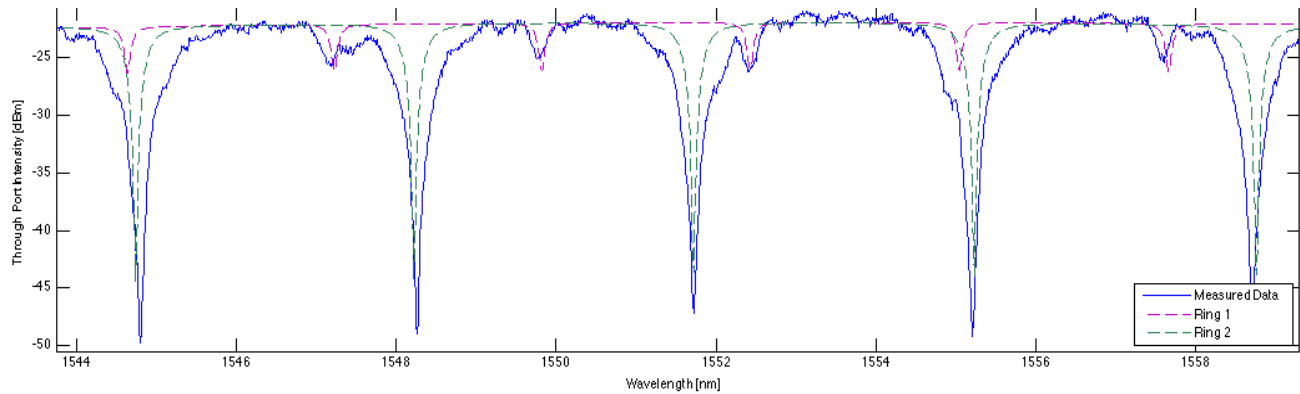


Figure 4. Simulated single-resonator responses overlaid upon the measured transmission spectrum for the cascaded two-resonator system. The FSR for the measured Ring 1 response is 2.61 ± 0.03 nm, whereas that for the simulated Ring 1 response is 2.61 ± 0.010 nm. The FSR for the measured Ring 2 response is 3.45 ± 0.014 nm, while that for the simulated response is 3.48 ± 0.015 nm.

The measured and simulated FSRs agree reasonably well for both rings. The small discrepancies are likely due to temperature differences or small inaccuracies in the simulated waveguide geometry (as there were inaccuracies in measuring the waveguide geometry from the SEM cross-sections).

3.4 Simulated Refractive Index Sensitivity

As expected, there was a linear relationship between the simulated effective indices for the each of the modes and the expected refractive index change. The plot of simulated effective index (at $\lambda=1500$ nm) vs. expected shift in medium refractive index for each of the modes is presented in Figure 5.

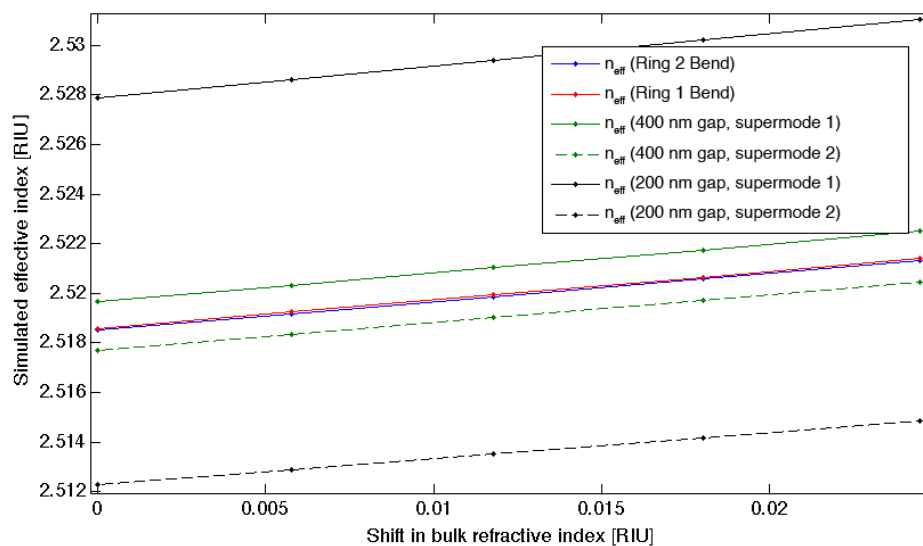


Figure 5. Simulated effective index (at $\lambda=1500$ nm) vs. bulk refractive index change, for the ring bend regions as well as the two supermodes for each of the two simulated coupler gaps.

4. RESULTS

The volume refractive index sensitivity of the racetrack resonator is determined by injecting a water – glycerin mixture with different mixing ratios and known refractive indices into the corresponding microchannels. The use of the cascaded resonators allows the measurement of individual resonators in different microchannels simultaneously with one frequency sweep.

4.1 Transmission Spectra

Figure 6 (a) and (b) show the through port transmission spectra and the center wavelength changes $\Delta\lambda_{\text{res}}$ for different racetrack resonators as a function of the water – glycerin concentration. Q-factors of $>40'000$ are measured for certain designs. Figure 6 (a) shows the measured transmission spectrum of two cascaded resonators. Both resonators are exposed individually to different environments. The first resonator (Ring 1) with an FSR of 2.9 ± 0.02 nm is immersed into DI water. The second resonator (Ring 2) with an FSR of 3.45 ± 0.014 nm is exposed to five different water – glycerin concentrations of 0, 5, 10, 15, 20 wt% (see Table 1 for the corresponding refractive indices). The refractive index in channel 1 does not change and therefore there is no resonance peak shift occurring. For Ring 2 the resonance peak shifts linearly with glycerin – water concentration or linearly with increasing refractive index. Similarly Figure 6 (b) shows the measured transmission spectrum of a four resonator system. Again, each resonator can be exposed individually to different environments. Here Ring 1, 2 and 4 are kept constant (exposed to DI water) and Ring 3 is immersed into water and a 10wt% glycerin – water solution respectively.

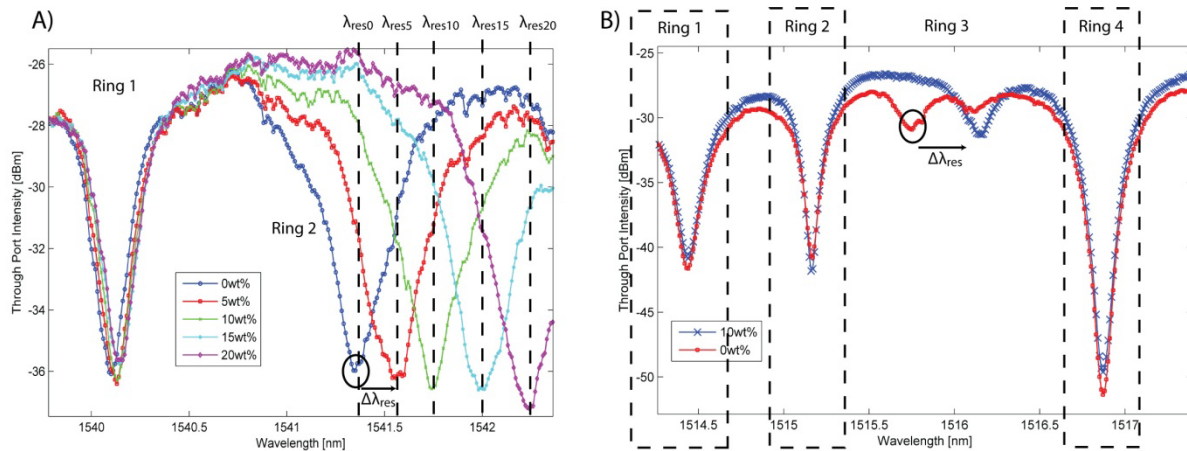


Figure 6: a) Transmission spectra for a 2 ring system. Ring 1 is exposed to DI water and Ring 2 is exposed to different water – glycerin mixtures. b) Transmission spectra for a 4 ring system. Ring 1,2, and 4 are exposed to DI water. Ring 3 is exposed to two different water-glycerin mixtures.

4.2 Refractive Index Sensitivity

For the two resonator system the net shift in resonance peak as a function of refractive index is depicted in Figure 7. The resonance peak for pure DI water for Ring 2 is at $\lambda_{\text{res}0} = 1541.35 \text{ nm} \pm 0.008 \text{ nm}$. For a refractive index change of $\Delta n = 0.02446$ which corresponds to a switch from DI water to a 20wt% glycerin – water solution the resonance peak shifts to $\lambda_{\text{res}20} = 1542.24 \text{ nm} \pm 0.01 \text{ nm}$. This corresponds to a sensitivity of $\sim 36 \text{ nm/refractive index unit (RIU)}$. The volume refractive index sensitivity shows a linear relationship. The linear curve fit parameters are $a = 36.6385$ and $b = 1492.5$ (for least square fit to $y=ax+b$). The obtained relationship is compared to the predictions from the finite element model. The diamond shaped data set in Figure 7 represents the modelled values. Despite the fact that the model overestimates the sensitivity, the measured results are sufficiently close to the predicted values, indicating that this model can be used for optimizing the design of the resonator geometries to further enhance Q-factors and sensitivity. The mode simulations (see Figure 3) show that only a small fraction of the field intensity of the optical mode propagates outside the waveguide and can therefore interact with the sample. The use of slotted waveguides would increase the fraction of power propagating outside the waveguide and therefore would increase the sensitivity. The finite element model computed using Lumerical MODE Solutions and a custom MATLAB script can easily be adapted to simulate slotted

waveguides as well. Other important parameters of the system not quantified in this work are the sensor resolution, i.e. the smallest possible spectral shift that can be accurately measured, and the detection limit, the minimum amount of sample analyte (or RIU change) that the sensor can quantify. They are dependent of the systems' spectral resolution and noise factors. In this work resonance peaks are detected by simply tracking the position of the minimum values in the transmission spectra thus making it very sensitive to noise. The measurement is done at steady state multiple times and the error bars in Figure 7 indicate the variation of the resonance peak. A better approach would be to approximate the resonant profiles by a Gaussian distribution and then compute the mean value and standard deviation.

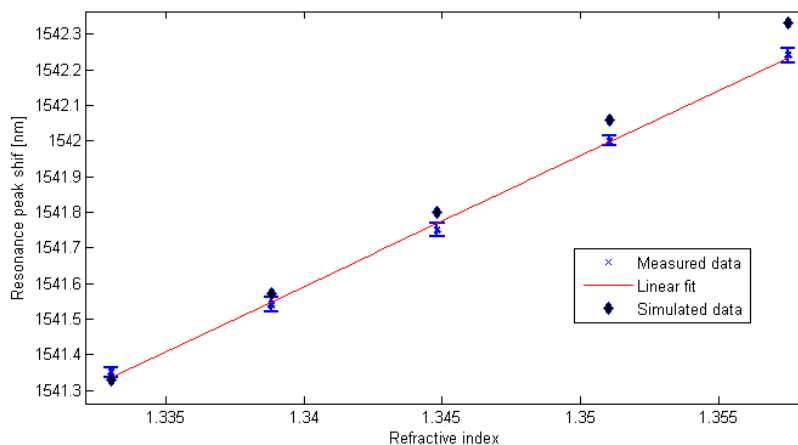


Figure 7: Resonance wavelength shift as a function of the refractive index of the binary mixture. The measured data is compared to the predicted values from the finite element model.

5. CONCLUSION

In summary, we proposed and implemented the use of cascaded ring resonators together with a PDMS microfluidic network fabricated by soft lithography to expose each ring individually to different solutions. We have shown that each resonator individually exposed to different environments can be simultaneously measured with one single wavelength sweep. The volume refractive index sensitivity of the racetrack resonator is determined by injecting a water – glycerin mixture with different mixing ratios and known refractive indices. Furthermore we have shown that we can accurately predict resonator properties by implementing a finite element model using Lumerical MODE Solutions and a custom MATLAB script

ACKNOWLEDGEMENTS

We would like to thank Dr. Li Yang from the Simon Fraser University (SFU) nano-imaging facility for kindly assisting with and providing training for the SEM/FIB used to measure the waveguide cross-sections. We would like to thanks as well Prof. Nicolas A. F. Jaeger from the University of British Columbia (UBC) for his insights and support. We are also grateful to Lumerical Solutions, Inc. for providing the simulation software and to CMC Microsystems for the assistance in the design of the mask layout.

REFERENCES

- [1] Washburn, A. L., Gunn, L. C. and Bailey, R. C., "Label-Free Quantitation of a Cancer Biomarker in Complex Media Using Silicon Photonic Microring Resonators," *Anal. Chem.*, 81, 9499-9506 (2009)
- [2] Little, B. E., Chu, S. T., Pan, W., Ripin, D., Kaneko, T., Kokubun, Y. and Ippen, E., "Vertically coupled glass microring resonator channel dropping filters," *IEEE Photo. Technol. Lett.*, 11, 215-217 (1999)
- [3] Kaalund, C. J., "Critically coupled ring resonators for add-drop filtering," *Opt. Comm.*, 237, 357-362 (2004)

- [4] Nielson, G. N., Seneviratne, D., Lopez-Royo, F., Rakich, P. T., Avrahami, Y., Watts, M. R., Haus, H. A., Tuller, H. L. and Barbastathis, G., "Integrated Wavelength-Selective Optical MEMS Switching Using Ring Resonator Filters," *IEEE Photon. Technol. Lett.*, 17, 1190-1192 (2005)
- [5] Zhixi, B., Ali, S., Bin, L. and Dominik, G. R., "Demonstration of semiconductor microring resonator coupled lasers," *Conf. on Lasers and Elec.-Opt.*, 2004.
- [6] Liu, B., Shakouri, A. and Bowers, J. E., "Passive microring-resonator-coupled lasers," *Appl Phys Lett*, 79, 3561-3563 (2001)
- [7] Yang, G. M., White, I. M. and Fan, X. D., "An opto-fluidic ring resonator biosensor for the detection of organophosphorus pesticides," *Sensor Actuat B-Chem*, 133, 105-112 (2008)
- [8] Passaro, V. M. N., Dell'Olio, F., Ciminelli, C. and Armenise, M. N., "Efficient Chemical Sensing by Coupled Slot SOI Waveguides," *Sensors-Basel*, 9, 1012-1032 (2009)
- [9] Ramachandran, A., Wang, S., Clarke, J., Ja, S. J., Goad, D., Wald, L., Flood, E. M., Knobbe, E., Hryniewicz, J. V., Chu, S. T., Gill, D., Chen, W., King, O. and Little, B. E., "A universal biosensing platform based on optical micro-ring resonators," *Biosens Bioelectron*, 23, 939-944 (2008)
- [10] Carlborg, C. F., Gylfason, K. B., Kazmierczak, A., Dortu, F., Polo, M. J. B., Catala, A. M., Kresbach, G. M., Sohlstrom, H., Moh, T., Vivien, L., Popplewell, J., Ronan, G., Barrios, C. A., Stemme, G. and van der Wijngaart, W., "A packaged optical slot-waveguide ring resonator sensor array for multiplex label-free assays in labs-on-chips," *Lab Chip*, 10, 281-290 (2010)
- [11] Luchansky, M. S. and Bailey, R. C., "Silicon Photonic Microring Resonators for Quantitative Cytokine Detection and T-Cell Secretion Analysis," *Anal. Chem.*, 82, 1975-1981 (2010)
- [12] Claes, T., Molera, J. G., De Vos, K., Schacht, E., Baets, R. and Bienstman, P., "Label-Free Biosensing With a Slot-Waveguide-Based Ring Resonator in Silicon on Insulator," *IEEE Photon. J.*, 1, 197-204 (2009)
- [13] Fan, X. D., White, I. M., Shopoua, S. I., Zhu, H. Y., Suter, J. D. and Sun, Y. Z., "Sensitive optical biosensors for unlabeled targets: A review," *Anal Chim Acta*, 620, 8-26 (2008)
- [14] Passaro, V. M. N., Dell'Olio, F., Casamassima, B. and De Leonardis, F., "Guided-wave optical biosensors," *Sensors-Basel*, 7, 508-536 (2007)
- [15] White, I. M. and Fan, X. D., "On the performance quantification of resonant refractive index sensors," *Opt Express*, 16, 1020-1028 (2008)
- [16] Baehr-Jones, T., Hochberg, M., Walker, C. and Scherer, A., "High-Q optical resonators in silicon-on-insulator-based slot waveguides," *Appl Phys Lett*, 86, - (2005)
- [17] Barrios, C. A., Banuls, M. J., Gonzalez-Pedro, V., Gylfason, K. B., Sanchez, B., Griol, A., Maquieira, A., Sohlstrom, H., Holgado, M. and Casquel, R., "Label-free optical biosensing with slot-waveguides," *Opt Lett*, 33, 708-710 (2008)
- [18] Barrios, C. A., Gylfason, K. B., Sanchez, B., Griol, A., Sohlstrom, H., Holgado, M. and Casquel, R., "Slot-waveguide biochemical sensor," *Opt Lett*, 32, 3080-3082 (2007)
- [19] Dell'Olio, F. and Passaro, V. M. N., "Optical sensing by optimized silicon slot waveguides," *Opt Express*, 15, 4977-4993 (2007)
- [20] Keivani, H. and Kargar, A., "Bending Efficiency of Bent Multiple-Slot Waveguides," *Chinese Phys Lett*, 26, 124204 (2009)
- [21] Boyd, R. W. and Heebner, J. E., "Sensitive disk resonator photonic biosensor," *Appl Optics*, 40, 5742-5747 (2001)
- [22] Gylfason, K. B., Carlborg, C. F., Kazmierczak, A., Dortu, F., Sohlstrom, H., Vivien, L., Barrios, C. A., van der Wijngaart, W. and Stemme, G., "On-chip temperature compensation in an integrated slot-waveguide ring resonator refractive index sensor array," *Opt Express*, 18, 3226-3237 (2010)
- [23] Kwon, M.-S. and Steier, W. H., "Microring-resonator-based sensor measuring both the concentration and temperature of a solution," *Opt. Express*, 16, 9372-9377 (2008)
- [24] Dai, D. X. and He, S. L., "Highly-sensitive sensor with large measurement range realized with two cascaded-microring resonators," *Opt Commun*, 279, 89-93 (2007)
- [25] Sumetsky, M., "Optimization of optical ring resonator devices for sensing applications," *Opt. Lett.*, 32, 2577-2579 (2007)
- [26] Ma, C.-S., Wang, X.-Y., Li, D.-L. and Qin, Z.-K., "Characteristic analysis of series-cascaded microring resonator arrays," *Opt. & Laser Technol.*, 39, 1183-1188 (2007)
- [27] Quake, S. R. and Scherer, A., "From micro- to nanofabrication with soft materials," *Science*, 290, 1536-1540 (2000)
- [28] Ksendzov, A. and Lin, Y., "Integrated optics ring-resonator sensors for protein detection," *Opt. Lett.*, 30, 3344-3346 (2005)

- [29] Rouger, N., Chrostowski, L. and Vafaei, R., "Temperature Effects on Silicon-on-Insulator (SOI) Racetrack Resonators: A Coupled Analytic and 2-D Finite Difference Approach," *J Lightwave Technol*, 28, 1380-1391 (2010)
- [30] Rabus, D. G., *Integrated Ring Resonators*, 1 edn., Springer, 2007.